Asymmetric stem cell division maintains the genetic heterogeneity of tissue cells

Muhammed Burak Bener[1], Boris M. Slepchenko[1, 2*] and Mayu Inaba[1*]

[1]Department of Cell Biology, University of Connecticut School of Medicine, Farmington, CT 06030
[2]Richard D. Berlin Center for Cell Analysis and Modeling, University of Connecticut School of Medicine, Farmington, CT 06030

[*] Correspondence: inaba@uchc.edu, boris@uchc.edu

ABSTRACT

Within a given tissue, the stem cell niche provides the microenvironment for stem cells suitable for their self-renewal. Conceptually, the niche space constrains the size of a stem-cell pool, as the cells sharing the niche compete for its space. It has been suggested that either neutral- or non-neutral-competition of stem cells changes the clone dynamics of stem cells. Theoretically, if the rate of asymmetric division is high, the stem cell competition is limited, thus suppressing clonal expansion. However, the effects of asymmetric division on clone dynamics have never been experimentally tested. Here, using the *Drosophila* germline stem cell (GSC) system, as a simple model of the in-vivo niche, we examine the effect of division modes (asymmetric or symmetric) on clonal dynamics by combining experimental approaches with mathematical modeling. Our experimental data and computational model both suggest that the rate of asymmetric division is proportional to the time a stem cell clone takes to expand. Taken together, our data suggests that asymmetric division is essential for maintaining the genetic variation of stem cells and thus serves as a critical mechanism for safeguarding fertility over the animal age or preventing multiple disorders caused by the clonal expansion of stem cells.

Introduction

In a tissue, stem cells reside in the specialized microenvironment for stem-cell maintenance called a niche. Within the niche, stem cells can divide both symmetrically and asymmetrically, and the proportion of these two division modes greatly varies among different stem cell systems[1]. Typically, a defect in asymmetric cell division (ACD) can lead to loss or gain of the number of stem cell and subsequent replacement or removal events mediated by symmetric cell division (SCD). So long as the replaced cells are genetically or phenotypically equivalent to the original stem cells, tissue defects may not occur. However, once a stem-cell clone gains a harmful mutation, the expansion of such a clone may lead to disruption of tissue homeostasis and initiation of a disease. In the case of germline stem cells, it directly affects genetic diversification or fertility, thus has a huge impact on animal evolution. So far, many studies have investigated the dynamics of stem cell clones, both with computational and experimental approaches[2-7]. However, the role of ACD has not been clearly demonstrated.

Surprisingly, potential beneficial effect of ACD on maintaining genetic heterogeneity have been overlooked by researchers. Irrelevant to the effect of ACD on clone expansion, dysregulation of call fate determination caused by ACD defect has been shown, which leads to tumorigenesis[8-14]. In contrast, ACD also has tumor-promoting effects. For example, ACD can produce phenotypically heterogenous cell populations in cancer, which leads to resistance for treatment[15,16]. Furthermore, the quality surveillance mechanism, such as the elimination of damaged stem cells from the tissue, relies on cell-cell competition promoted by SCD[17-19]. Quantitative analysis of stem cell behavior in the real niche is necessary to revisit and evaluate the roles of ACD in tissue homeostasis.

Studying the *Drosophila* GSC system has yielded valuable information for our understanding of many conserved stem-cell characteristics. At the tip of the *Drosophila* testis, 8-10 GSCs adhere to a cluster of somatic cells called the hub, a major niche component. The hub cells send signals which are vital for GSC maintenance. In this microenvironment, GSCs typically divide asymmetrically via a stereotypical spindle orientation. This ACD results in only one daughter cell maintaining attachment to the hub and retaining its stem cell identity, and a second daughter cell is displaced away from the hub and becomes a gonialblast (GB) that begins to differentiate[12,20] (Figure 1A).

Owing to its simple and well-characterized tissue anatomy and defined cellular markers, this model is especially suited to addressing the impact of ACD defects on the clonal expansion rate of stem cells using both computational and experimental approaches.

Results

Asymmetric cell division delays the clone expansion.

To assess the role of ACD on the clonal expansion of stem cells within normal tissue homeostasis, we have conducted a simulation of the dynamics of stem-cell clones in the testicular niche using the Virtual Cell (VCell) platform[21,22]. At first, we generated a geometry of the virtual niche by mimicking the real GSC niche in Drosophila testis. The niche capacity is constantly adjusted to maintain 9 plus/minus 1 cells that are dividing non-synchronously every 12 hours (Figure 1B). This assumption is based on the knowledge that the GSC number is strictly controlled depending on available niche space.

We defined the "clonal niche" as the niche occupied by a single clone. Next, we simulated the frequency of emergence of clonal niche for cases in which GSCs divide with various probabilities of ACD (p) and SCD (symmetric self-renewal (q), and symmetric differentiation (r)), with the constraints that are q=r and p+q+r=1 (Figure 1C). Each stem cell clone, labelled A1 through A9, was assigned identical rates of p, q, and r, and represented by unique colors in the simulation outputs. We conducted 3,000 simulations for each set of parameters (model i through v) and recorded the number of each stem cell clone after every cell division event occurring in the virtual niche (Figure 1D).

Representative single trials from each parameter set (model i through v) are shown in Figure 1E-I. The cumulative probabilities of single-clone expansion for models i through v demonstrate how the different probabilities of ACD (p), SCD (symmetric self-renewal, q) and SCD (symmetric differentiation, r) influence clonal dynamics within the niche (Figure 1J).

Strikingly, our simulation result revealed the relationship between the time taken for the emergence of clonal niches and the rate of ACD (Figure 1K) is proportional. These models demonstrate that ACD has a delaying effect on the onset of clonal expansion of stem cells.

Fitting with experimental results using *Drosophila* germline stem cells

Next, we conducted two lineage tracing experiments (long-term and short-term) in *Drosophila* testis to monitor the clone dynamics in vivo. To permanently mark the GSC clones by GFP, we induced Flippase expression (hs-FLP) by incubating flies in 37 degrees for short time (heat shock), which removes the stop codon located between nanos promoter and Gal4, thereby initiating the UAS-GFP expression (Figure 2A)[23]. We optimized the heat-shock duration to 40 minutes to mark approximately 50% of the GSCs (Figure 2B). We then followed the frequency of GFP-positive GSCs at day 7, 14, and 21 days post-marking. If GSCs always divide asymmetrically (p=1), the GFP-positive clone frequency should remain around 50%. However, if symmetric events occur, the GFP-positive GSC frequency will be biased towards 0% or 100% (Figure 2C). During our imaging period, we observed a shift in GFP-positive GSC frequency towards these trends (Figure 2D). The speed of the change in GFP-positive GSC frequency will

tell us the probability of ACD. To accurately determine the ACD rate (p and q= r values), we have fitted our model to the experimental data. We ran 2,000 simulations for each set of parameters: 1) p=0.9, q=r=0.05, 2) p=0.8, q=r=0.1, and 3) p=0.7, q=r=0.15. We found that the model with p=0.8, q=r=0.1, fitted best to our experiment results (Figure 2E). This finding was consistent with both a previous study, and our prior data[24,25].

We realized that this rate is somewhat inconsistent with a previous report which estimated ACD rate by analyzing distribution pattern of the GFP-positive clones (Figure 3A). Under the assumption that symmetric stem cell division creates two GFP-positive GSCs that are juxtaposed to each other (doublet), ACD and SCD rates were estimated. In this study, ACD rate was estimated 94-98% (p=0.94~0.98)[23]. To consider possible reason of the gap between two studies, we first repeated same quantification and we consistently saw very similar pattern of marked cells to what was shown in the previous study (Figure 3B). However, we realized that the estimated "symmetric events" in this study do not contain the of "dedifferentiation" events. As expected, the gap between ~95% and ~80% exactly matches to the estimated dedifferentiation frequency (15%)[26], indicating that the overall frequency of asymmetric outcomes with consideration of the rate of dedifferentiation is most likely ~80%.

Discussion

Tissue stem cells reside in specialized microenvironments called the niche. Traditionally, it has been believed that asymmetric division is the primary mechanism for stem cell maintenance by balancing self-renewal and differentiation. However, the niche is constrained in size, leading to continuous competition among stem cells for space through a neutral drift. Consequently, the stem cells can also be maintained through symmetric divisions without expansion or reduction. In most tissues, both asymmetric and symmetric divisions contribute to stem cell maintenance. Importantly, the role of asymmetric divisions for the long-term tissue homeostasis has often been overlooked.

In this study, we found that a niche with a high probability of ACD (p>0.9) never reaches a clonal niche (the condition in which a niche is occupied by a single clone) within the average lifetime of flies (~120 divisions, equivalent to ~60 days) [27,28]. In contrast, a low probability of ACD (p<0.4) results in a niche that quickly becomes clonal (~22 divisions, 11 days, Figure 1E-I), supporting our hypothesis that ACD is an essential factor for preventing clone expansion.

Our findings provide significant insights on clonal dynamics of stem cells and suggests potential therapeutic strategies that could manipulate the division modes of stem cells to suppress clonal expansion in disease conditions. Furthermore, the mathematical model used in this study could be adapted to predict stem cell behavior in mammalian stem cell niches, across both steady-state and various pathological

conditions.

In recent years, clonal expansion of stem cells has emerged as a crucial factor in the development of multiple pathological conditions. Clonal hematopoiesis (CH) is a condition characterized by the presence of clonally expanded hematopoietic stem cells (HSCs) and has emerged as a risk factor for hematopoietic malignancy and cardiovascular diseases [29,30]. Extensive clinical studies have identified multiple commonly mutated genes within these expanding HSC clones and explored the mechanisms by which these mutations contribute to disease progression [29,31]. Removal of mutant clones by manipulating competition between mutant and normal cells has been suggested as a novel strategy of definitive treatment [32-39], but much of mechanistic knowledge required for implementation of such treatment is still lacking.

Materials and methods

Fly husbandry and strains

All fly crosses were performed on standard Bloomington medium at 22°C to avoid hs-flp expression and indicated age (days after clone marking) of flies were used for all experiments. The following fly stocks were obtained from Bloomington stock center (BDSC); *hs-flp* (BDSC1929). nos-FRT-mCherry-stop-FRT-Gal4, UAS-GFP [40] was from Inaba lab stock.

GFP labeling of germline stem cells

Flies carrying the heat-shock-FLP allele were crossed with nos-FRT-mCherry-stop-FRT-Gal4, UAS-GFP flies and maintained at 22°C. 0-3 days old progenies were heat-shocked in a 37°C water bath once for 40 min (optimized for 50% marking) in vials with fly food. Vials were placed back at 22°C and testes were dissected at desired time points (24hrs, day7, 14 and 21 post-heatshock).

Immunofluorescence Staining

Testes were dissected in phosphate-buffered saline (PBS) and fixed in 4% formaldehyde in PBS for 30–60 minutes. Next, testes were washed in PBST (PBS + 0.2% TritonX-100, Thermo Fisher) for at least 60 minutes, followed by incubation with primary antibody in 3% bovine serum albumin (BSA) in PBST at 4°C overnight. Samples were washed for 60 minutes (three times for 20 minutes each) in PBST, incubated with secondary antibody in 3% BSA in PBST at room temperature for 2 hours and then washed for 60 minutes (three times for 20 minutes each) in PBST. Samples were then mounted using VECTASHIELD with 4’,6-diamidino-2-phenylindole (DAPI) (Vector Lab).
The primary antibodies used were as follows: rat anti-Vasa (1:20; developed by A. Spradling and D. Williams, obtained from Developmental Studies Hybridoma Bank (DSHB); mouse anti-Hts (1B1, 1:20;

DSHB) mouse-anti-FasIII (1:20, 7G10; DSHB); AlexaFluor-conjugated secondary antibodies (Abcam) were used at a dilution of 1:400.

Mathematical modeling

To study dynamics of unsynchronized clones, we formulate a continuous-time stochastic model. We first assume that all clones are described by same probability rates of outcomes of randomly occurring asymmetric and symmetric divisions, thus, there are three model parameters: the rate constant of asymmetric division p, and the rate constants of symmetric self-renewal q and symmetric differentiation r.

Let ν be the division frequency, then $p + q + r = \nu$. Because cell cycle duration of stem cells sets the model time scale, it is convenient to use it as a time unit, then $\nu = 1\left(\frac{1}{\text{cycle}}\right)$ and $p + q + r = 1(\frac{1}{\text{cycle}})$. Since the average number of cells in the niche is constant, then q must equal r, so the system has only one independent parameter. However, even with $q = r$, fluctuations of the niche population around its average size would grow with time, unless additional regulation is exercised, as described below.

Our model is formulated in terms of numbers of descendants of individual clones $\{n_i\}$, where index i enumerates original clones (and their descendants): $i = 1, \dots, N$, where N is the niche capacity. The dynamics of n_i are governed by the randomly occurring events of asymmetric and symmetric divisions.

To restrict fluctuations of the population size, the niche must ensure that the total number of cells, n_{tot}=$\sum_1^N n_i$, at any time remains close to N: $|n_{\text{tot}} - N| < \varepsilon$, where ε is a small positive integer. Care must be taken to interpret such control in a biologically consistent manner (see detailed discussion later in this section). Our implementation of the tight control over n_{tot} by the niche assumes a strong correlation between the proliferation and differentiation occurrences. Specifically, the system is governed by the following transition probabilities:

$$P(n_i, t + dt|\, n_i, t) = p n_i dt \qquad \text{(clone maintenance);}$$

$$P(n_i + 1, t + dt|\, n_i, t) = n_i\, dt \times \begin{cases} q, & \text{if } N - \varepsilon < n_{\text{tot}} < N + \varepsilon \\ q + r, & \text{if } n_{\text{tot}} = N - \varepsilon \end{cases} \text{(clone proliferation);} \qquad \text{Eqs (1)}$$

$$P(n_i - 1, t + dt|\, n_i, t) = n_i\, dt \times \begin{cases} r, & \text{if } N - \varepsilon < n_{\text{tot}} < N + \varepsilon \\ q + r, & \text{if } n_{\text{tot}} = N + \varepsilon \end{cases} \text{(clone differentiation).}$$

The model was solved by generating stochastic trajectories of the system in *Virtual Cell* [21] with a nonspatial Monte Carlo solver based on the Gibson - Bruck method [41]. The clonal expansion was analyzed for the uniform initial conditions, $n_i|_{t=0} = 1$ for all $i = 1, \dots, N$. Results indicate that our model retains features of discrete-time Moran-type stochastic processes [42,43], with all n_i being interdependent.

Note that the inequality $|n_{\text{tot}} - N| < \varepsilon$ can also be enforced by lowering transition probabilities of the symmetric outcomes that violate this inequality or setting such probabilities to zero. Below is an example of postulating low probabilities of unwanted symmetric outcomes:

$$P(n_i + 1, t + dt|\, n_i, t) \;= n_i\, dt \cdot f(n_{\text{tot}}) \;\text{ (clone proliferation)},$$
$$P(n_i - 1, t + dt|\, n_i, t) = n_i\, dt \cdot (1 - f(n_{\text{tot}})) \;\text{ (clone differentiation)}, \qquad \text{Eqs (2)}$$

with $f(n_{\text{tot}}) = (1 + (n_{\text{tot}}/N)^{10})^{-1}$ [43].

Alternatively, the probabilities of the outcomes violating the limits for n_{tot} could be set to zero:

$$P(n_i + 1, t + dt|\, n_i, t) \;= n_i\, dt \times \{\begin{matrix} 1, \text{ if } n_{\text{tot}} \leq N + \varepsilon - 1 \\ 0, \quad \text{otherwise} \end{matrix} \;\text{ (clone proliferation)},$$
$$P(n_i + 1, t + dt|\, n_i, t) \;= n_i\, dt \times \{\begin{matrix} 1, \text{ if } n_{\text{tot}} \geq N - \varepsilon + 1 \\ 0, \quad \text{otherwise} \end{matrix} \;\text{ (clone differentiation)}. \qquad \text{Eqs (3)}$$

(The transition probability of asymmetric divisions in these approaches is the same as in Eqs (1)).

These models, however, result in an artificial dependence of a cell cycle period on the type of division the stem cell decides to undergo (Figure 2). Indeed, because these methods effectively rule out certain symmetric outcomes, there are on average fewer symmetric divisions per unit time than asymmetric ones. As a result, the average period of a symmetric division is longer than that of an asymmetric one.

Such an artefact does not arise in the model defined by Eqs (1).

Utilizing the mathematical model for analyzing experimental data

We used the mathematical model described in the previous section for analyzing data obtained in experiments with transgenic male flies that enable induction of GFP-labeled stem cell clones. The experiments were aimed at determining the values of p, q and r characteristic of the population dynamics of GSCs in Drosophila testes.

An earlier study of clone expansion in transgenic flies estimated fractions of symmetric divisions to be in the range of 1 to 2% {Salzmann, 2013 #13}. The estimate was obtained by comparing fractions of various numbers of GFP-marked cells per niche, observed over time, with predictions from a mathematical model. The applicability of the model used in the study is limited to experiments with niches having only few GFP-positive cells at any time, because it ignores the effect of symmetrically dividing unmarked cells on dynamics of marked cells (given that the total number of GSCs in the niche, marked and unmarked, is kept constant). In such experiments, the sum of marked cells over all inducted flies gradually diminishes due to differentiation. Neglecting this when computing predicted fractions of various numbers of marked

cells per niche would yield substantially underestimated rates of symmetric divisions. Also, amassing statistically significant data from experiments with small number of GFP-positive cells per niche requires examining large pools of flies and thus is inefficient.

In our experiments, the flies were inducted to have initial numbers of marked stem cells of about half the niche capacity. As in [5], we tracked over time fractions of GFP-positive cells in the niches, $\frac{n_{GFP+}}{N}$. Specifically, four portions of a large pool of inducted flies were sacrificed at times separated by seven days, with time zero being the closest to the time of induction. For each time point, testes were dissected, the total number of stem cells and the number GFP-positive cells were counted, and their ratio $\frac{n_{GFP+}}{N}$ was computed for each testis. The value of p was determined by comparing experimental distributions of $\frac{n_{GFP+}}{N}$ at the specific times t, $P_{\text{exp}}\left(\frac{n_{GFP+}}{N} \mid t\right)$, to corresponding distributions $P_{\text{theor}}\left(\frac{n_{GFP+}}{N} \mid t\right)$ predicted for varying p by the model whose applicability was not limited to small n_{GFP+} .

The predicted distribution was derived from multiple stochastic trajectories generated by a Monte Carlo simulator from Eqs (1) (see the previous section). In a single run, the solver returns an instance of n_{GFP+} at time t for a given N and an initial value of n_{GFP+} (in all calculations, we used $\varepsilon = 1$ and assumed that N does not change with time). Because in the experiments N varies from subject to subject, the predicted distribution $P_{\text{theor}}\left(\frac{n_{GFP+}}{N} \mid t\right)$ is a weighted average of the distributions obtained for each N experimentally observed at time t, and each n_{GFP+} observed at $t = 0$ that does not exceed the given N.

Accordingly, we first determined, by statistically processing the experimental results for each time point t, the frequencies, or 'weights', of all values of N observed at time t, $w_{exp}(N, t)$. Similarly, we determined the frequencies of all initial n_{GFP+} for each N observed at time t, $w_{exp}(n_{GFP+}, 0|N, t)$. Both weights were normalized to unity.

Secondly, for each pair of N and initial n_{GFP+}, we determined the probability distribution of $\frac{n_{GFP+}}{N}$ at a time point t, $P(\frac{n_{GFP+}}{N}, t|(N, t), (n_{GFP+}, 0))$. For this, we simulated large amounts of predicted n_{GFP+} by running the Monte Carlo solver with Eqs (1). Then the predicted distribution was computed as

$$\mathrm{P}_{\text{theor}}\left(\frac{n_{GFP+}}{N}, t\right)=\sum_{(N,t)}\{w_{exp}(N, t)[\sum_{(n_{GFP+},0)} w_{exp}(n_{GFP+}, 0|N, t)P(\frac{n_{GFP+}}{N}, t|(N, t), (n_{GFP+}, 0))]\}.$$

Note that one stochastic trajectory of the model with the uniform initial values: $n_i|_{t=0} = 1$ for all $i = 1, \dots, N$, yields $\binom{N}{m}$ instances of n_{GFP+} at time t, where m denotes the number of the GFP-positive cells at $t = 0$, $m = (n_{GFP+}, 0)$, and $\binom{N}{m} = \frac{N!}{m!(N-m)!}$. This is because every combination of m variables out of the total of N yields one instance of n_{GFP+} at time t. Alternatively, the model could be equivalently

rewritten in terms of only two variables $\{n_{0,}\, n_1\}$ denoting, respectively, the numbers of the GFP-negative and GFP-positive cells in the niche. Eqs (1) still apply, and N retains the meaning of niche capacity, but $i = 1{,}2$ and $n_{\text{tot}} = n_0 + n_1$. For this version of the model, one stochastic trajectory yields exactly instance of n_{GFP+} at time t.

For each time point and for each tested value of parameter p, we compared $P_{\text{exp}}\left(\frac{n_{GFP+}}{N} \mid t\right)$ and $P_{\text{theor}}\left(\frac{n_{GFP+}}{N} \mid t\right)$ by computing the root mean squared deviations,

$$\delta = \left(\frac{1}{M}\sum_{(n_{GFP+},\ t)}\left(P_{\text{exp}}\left(\frac{n_{GFP+}}{N} \mid t\right) - P_{\text{theor}}\left(\frac{n_{GFP+}}{N} \mid t\right)\right)^2\right)^{1/2},$$

where M is the number of values of $\left(\frac{n_{GFP+}}{N} \mid t\right)$ for which the probabilities were computed.

Statistical analysis and graphing

No statistical methods were used to predetermine sample size. The experiment values were not randomized. The investigators were not blinded to allocation during experiments and outcome assessment. Statistical analysis and graphing were performed using GraphPad prism9. All data are shown as means ± s.d. The adjusted P values from Šidák's multiple comparisons test are provided; shown as *P<0.05, **P<0.01, ***P<0.001, ****P<0.0001; NS, non-significant (P≥0.05).

Supplemental Data Individual numerical values displayed in all graphs are provided.

Acknowledgements

We thank Yukiko M. Yamashita and the Bloomington *Drosophila* Stock Center and the Developmental Studies Hybridoma Bank for reagents. This research is supported by R35GM128678 from National Institute for General Medical Sciences and start-up funds from UConn Health (to M.I.).

Author Contributions

All authors contributed equally for conception and design, interpretation of data and wrote and edited the manuscript. B.M.S conducted mathematical modeling and data fitting using Virtual Cell. M.B.B and M.I.; acquisition and analysis of experimental data.

Declaration of Interests

The authors declare no competing interests.

Figures

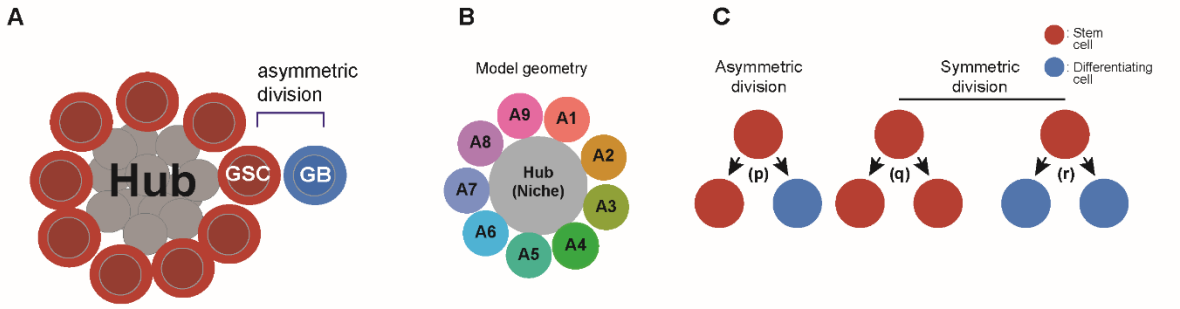

D

Standard parameters	Model (i)	Model (ii)	Model (iii)	Model (iv)	Model (v)
Stem cell number (n)	9±1	9±1	9±1	9±1	9±1
Asymmetric division (p)	0.96	0.9	0.8	0.6	0.4
Symmetric self-renewal (q)	0.02	0.05	0.1	0.2	0.3
Symmetric differentiation (r)	0.02	0.05	0.1	0.2	0.3

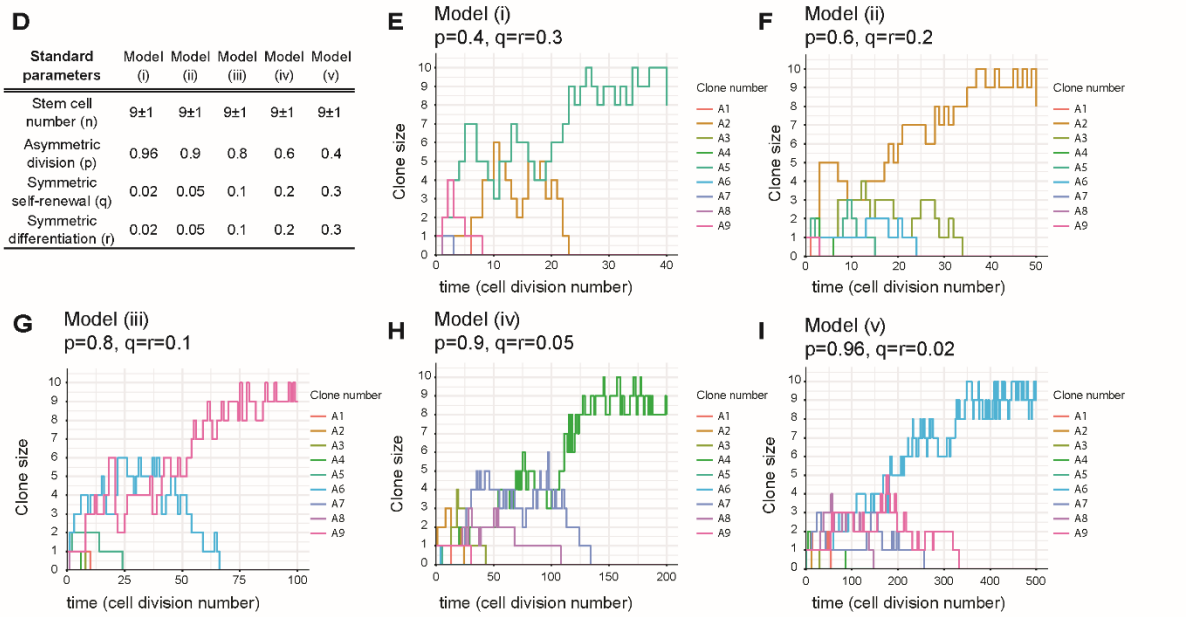

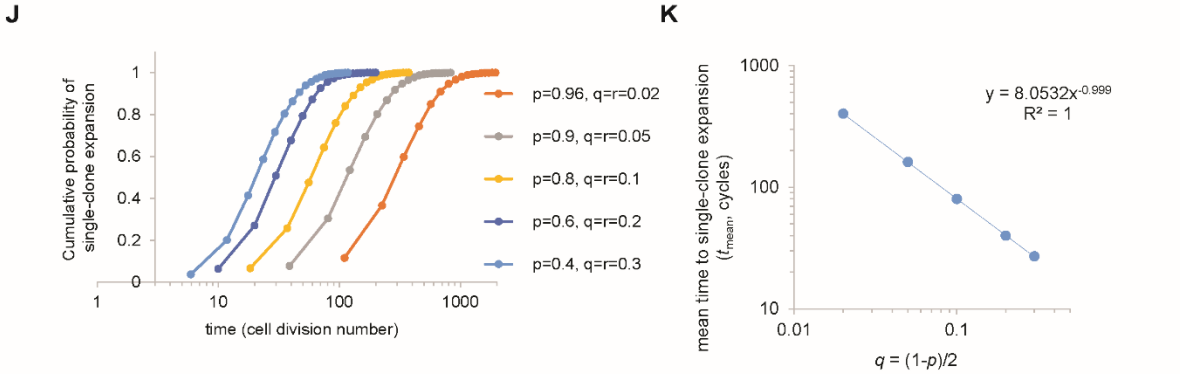

Figure 1. The effect of asymmetric cell division on stem cell clonality.

A) A schematic of the hub in the *Drosophila* testis.

B) The geometry of the hub introduced to the model. Stem cell clones are labeled A1 through A9.

C) Illustration of three potential outcomes of a stem cell division: asymmetric cell division (p), symmetric self-renewal (q) and symmetric differentiation (r).

D) Standard parameters for models i through v, including stem cell number (n) and division probabilities (asymmetric: p, symmetric: q and r).

E-I) For each model (i through v), a single representative trial that most closely matched the median number of cell cycles required for a single clone to dominate the niche was plotted to graphs.

J) Cumulative probability graph of single-clone expansion over the total number of cell cycles.

K) A graph showing the inverse relationship between the mean time to single-clone expansion and the rate of symmetric self-renewal (q).

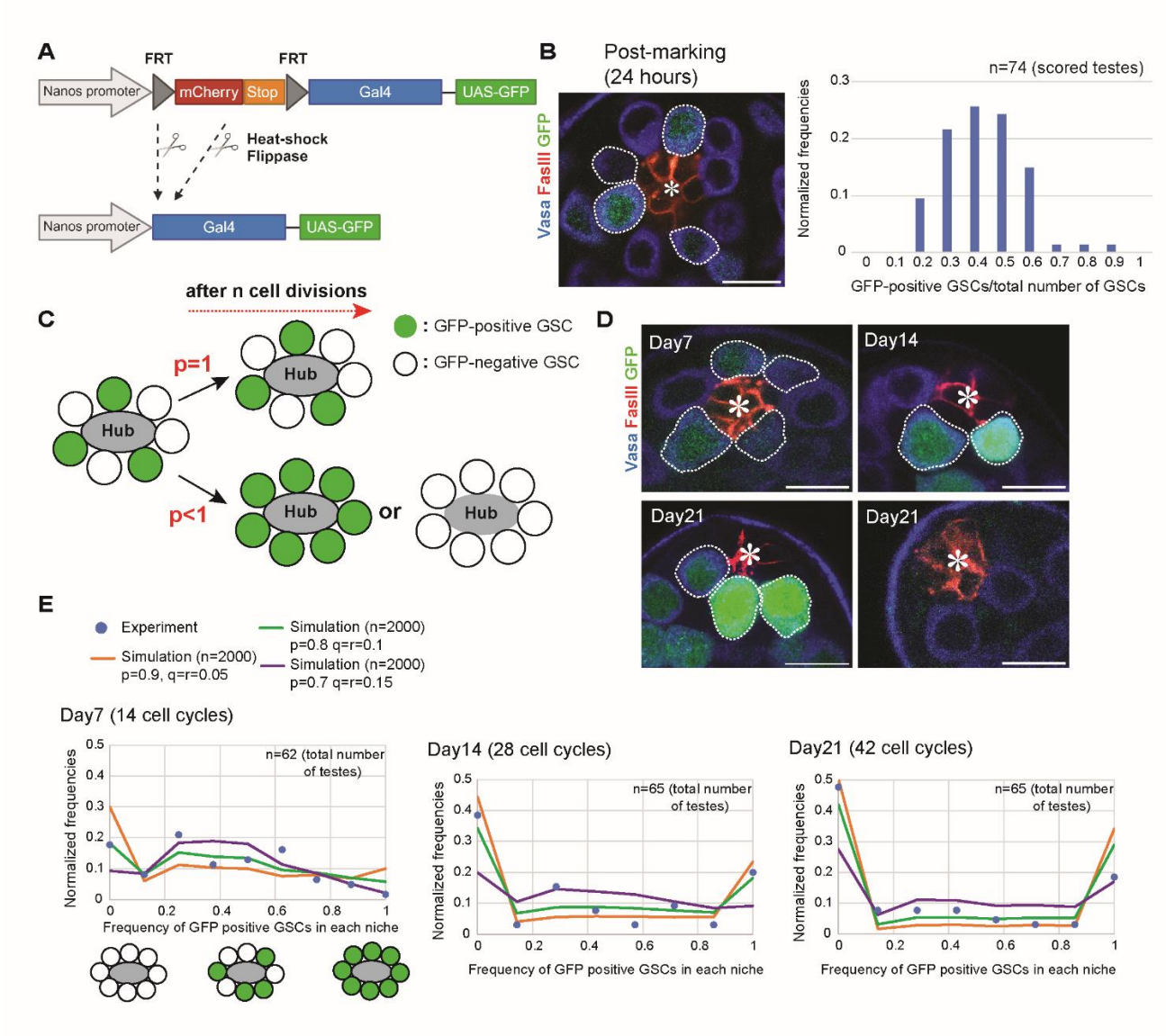
A
FRT
FRT
Nanos promoter
mCherry
Stop
Gal4
UAS-GFP
Heat-shock
Flippase
Nanos promoter
Gal4
UAS-GFP
B
Post-marking
(24 hours)
Vasa FasIII GFP
n=74 (scored testes)
Normalized frequencies
GFP-positive GSCs/total number of GSCs
C
after n cell divisions
: GFP-positive GSC
: GFP-negative GSC
p=1
p<1
Hub
or
D
Vasa FasIII GFP
Day7
Day14
Day21
Day21
E
Experiment
Simulation (n=2000)
p=0.9, q=r=0.05
Simulation (n=2000)
p=0.8 q=r=0.1
Simulation (n=2000)
p=0.7 q=r=0.15
Day7 (14 cell cycles)
n=62 (total number of testes)
Day14 (28 cell cycles)
n=65 (total number of testes)
Day21 (42 cell cycles)
n=65 (total number of testes)
Normalized frequencies
Frequency of GFP positive GSCs in each niche

Figure 2. Long-term clonal tracing of germline stem cells.

A) An illustration of the marking system. The heat-shock driven UAS-FLP expression removes the mCherry-stop cassette, and activate the expression of GFP in GSCs under the control of nosGal4.

B) Representative immunofluorescence image of the testicular niche 24 hours after a 40-minute of heat-shock. The graph shows the marking efficiency. Note that, the testes with no marked GSCs were excluded from the day0, and a proportionate number of unmarked testes were similarly excluded from the subsequent time points (day7, 14 and 21) (see details in "Mathematical modeling" in the Method section).

C) An illustration demonstrates expected results after marking 50% of GSCs. If GSCs exclusively undergo asymmetric division (p=1), the frequency of GFP-positive clones would remain around 50%. Conversely, if symmetric events occur, the distribution of GFP-positive GSCs within each testis would be biased towards 0% or 100% per testis.

D) Representative immunofluorescence images of the testicular niche at day7, 14 and 21. The upper panel shows images where the proportion of GFP-positive GSCs reaches 100%. In contrast, the lower panel shows images where the GFP-positive GSCs decline to 0%.

E) The graphs show the fitting of model to the experimental data. 2,000 simulations for each set of parameters were run: 1) p=0.9, q=r=0.05, 2) p=0.8, q=r=0.1, and 3) p=0.7, q=r=0.15. Root-mean-square deviation (RMSD) for each parameter set and its fit to the experimental data is indicated on the graph.

"n" indicates the number of imaged testes. All scale bars represent 10 μm. Asterisks in the images indicate the approximate location of the hub (niche).

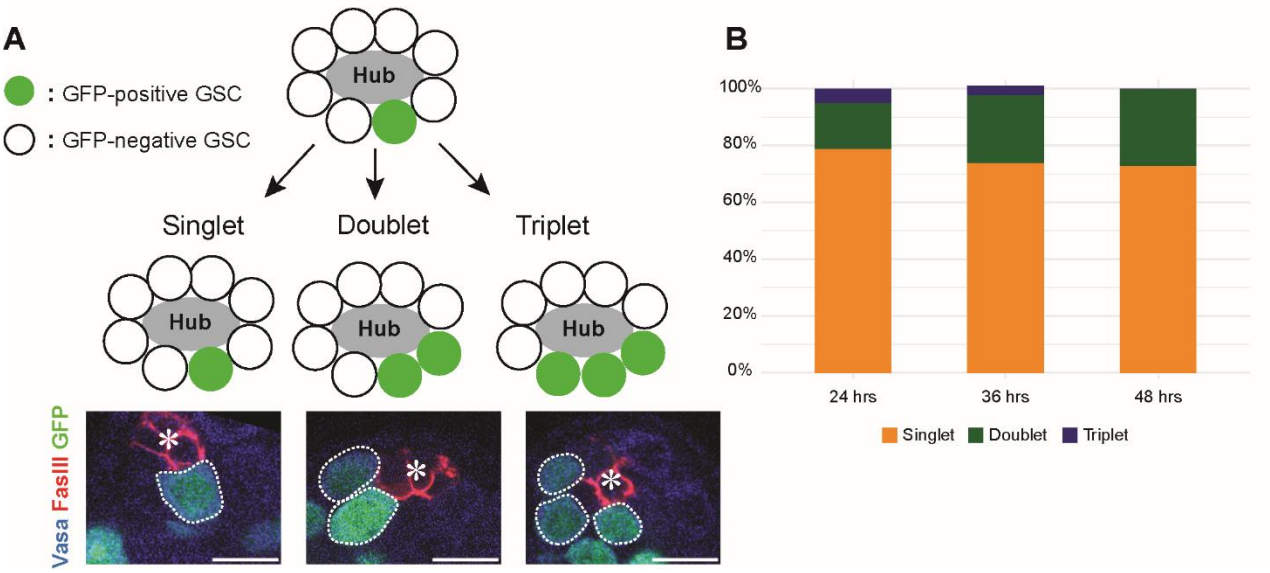

Figure 3. Short-term lineage tracing of germline stem cells.

A) Examples of singlet, doublet, and triplet GSCs 24 hours post-heat-shock treatment (30 mins) that has been optimized to mark ~1 GSC per testis. Representative immunofluorescence images of the singlet, doublet, and triplet examples. The singlet is observed when the marked GSC divides asymmetrically. The doublet and triplet are observed when the marked GSC undergoes symmetric self-renewal.

B) The graph illustrates the percentage of singlet, doublet, and triplet GSCs at 24-, 36- and 48-hours post-heat-shock treatment.

"n" indicates the number of imaged testes. All scale bars represent 10 μm. Asterisks in the images indicate the approximate location of the hub (niche).

References

1 Morrison, S. J. & Kimble, J. Asymmetric and symmetric stem-cell divisions in development and cancer. *Nature* **441**, 1068-1074 (2006). https://doi.org/10.1038/nature04956

2 Wallenfang, M. R., Nayak, R. & DiNardo, S. Dynamics of the male germline stem cell population during aging of Drosophila melanogaster. *Aging Cell* **5**, 297-304 (2006). https://doi.org/https://doi.org/10.1111/j.1474-9726.2006.00221.x

3 Clayton, E. *et al.* A single type of progenitor cell maintains normal epidermis. *Nature* **446**, 185-189 (2007). https://doi.org/10.1038/nature05574

4 Klein, A. M., Nakagawa, T., Ichikawa, R., Yoshida, S. & Simons, B. D. Mouse germ line stem cells undergo rapid and stochastic turnover. *Cell Stem Cell* **7**, 214-224 (2010). https://doi.org/10.1016/j.stem.2010.05.017

5 Lopez-Garcia, C., Klein, A. M., Simons, B. D. & Winton, D. J. Intestinal stem cell replacement follows a pattern of neutral drift. *Science* **330**, 822-825 (2010). https://doi.org/10.1126/science.1196236

6 Snippert, H. J. *et al.* Intestinal crypt homeostasis results from neutral competition between symmetrically dividing Lgr5 stem cells. *Cell* **143**, 134-144 (2010). https://doi.org/10.1016/j.cell.2010.09.016

7 de Navascués, J. *et al.* Drosophila midgut homeostasis involves neutral competition between symmetrically dividing intestinal stem cells. *Embo j* **31**, 2473-2485 (2012). https://doi.org/10.1038/emboj.2012.106

8 Lee, M. & Vasioukhin, V. Cell polarity and cancer – cell and tissue polarity as a non-canonical tumor suppressor. *Journal of Cell Science* **121**, 1141-1150 (2008). https://doi.org/10.1242/jcs.016634

9 Mukherjee, S., Kong, J. & Brat, D. J. Cancer stem cell division: when the rules of asymmetry are broken. *Stem Cells Dev* **24**, 405-416 (2015). https://doi.org/10.1089/scd.2014.0442

10 Wodarz, A. & Gonzalez, C. Connecting Cancer to the Asymmetric Division of Stem Cells. *Cell* **124**, 1121-1123 (2006). https://doi.org/10.1016/j.cell.2006.03.004
11 Betschinger, J., Mechtler, K. & Knoblich, J. A. Asymmetric Segregation of the Tumor Suppressor Brat Regulates Self-Renewal in Drosophila Neural Stem Cells. *Cell* **124**, 1241-1253 (2006). https://doi.org/10.1016/j.cell.2006.01.038
12 Yamashita, Y. M., Jones, D. L. & Fuller, M. T. Orientation of asymmetric stem cell division by the APC tumor suppressor and centrosome. *Science* **301**, 1547-1550 (2003). https://doi.org/10.1126/science.1087795
13 Ohshiro, T., Yagami, T., Zhang, C. & Matsuzaki, F. Role of cortical tumour-suppressor proteins in asymmetric division of Drosophila neuroblast. *Nature* **408**, 593-596 (2000). https://doi.org/10.1038/35046087
14 Peng, C. Y., Manning, L., Albertson, R. & Doe, C. Q. The tumour-suppressor genes lgl and dlg regulate basal protein targeting in Drosophila neuroblasts. *Nature* **408**, 596-600 (2000). https://doi.org/10.1038/35046094
15 Hitomi, M. *et al.* Asymmetric cell division promotes therapeutic resistance in glioblastoma stem cells. *JCI Insight* **6** (2021). https://doi.org/10.1172/jci.insight.130510
16 Dey-Guha, I. *et al.* Asymmetric cancer cell division regulated by AKT. *Proceedings of the National Academy of Sciences* **108**, 12845-12850 (2011). https://doi.org/doi:10.1073/pnas.1109632108
17 Ayukawa, S. *et al.* Epithelial cells remove precancerous cells by cell competition via MHC class I–LILRB3 interaction. *Nature Immunology* **22**, 1391-1402 (2021). https://doi.org/10.1038/s41590-021-01045-6
18 Wagstaff, L. *et al.* Mechanical cell competition kills cells via induction of lethal p53 levels. *Nature Communications* **7**, 11373 (2016). https://doi.org/10.1038/ncomms11373
19 Ji, Z., Chuen, J., Kiparaki, M. & Baker, N. Cell competition removes segmental aneuploid cells from Drosophila imaginal disc-derived tissues based on ribosomal protein gene dose. *eLife* **10**, e61172 (2021). https://doi.org/10.7554/eLife.61172
20 Venkei, Z. G. & Yamashita, Y. M. Emerging mechanisms of asymmetric stem cell division. *J Cell Biol* **217**, 3785-3795 (2018). https://doi.org/10.1083/jcb.201807037
21 Slepchenko, B. M. & Loew, L. M. Use of virtual cell in studies of cellular dynamics. *Int Rev Cell Mol Biol* **283**, 1-56 (2010). https://doi.org/10.1016/s1937-6448(10)83001-1
22 Resasco, D. C. *et al.* Virtual Cell: computational tools for modeling in cell biology. *Wiley Interdiscip Rev Syst Biol Med* **4**, 129-140 (2012). https://doi.org/10.1002/wsbm.165
23 Theodosiou, N. A. & Xu, T. Use of FLP/FRT system to study Drosophila development. *Methods* **14**, 355-365 (1998). https://doi.org/10.1006/meth.1998.0591
24 Bener, M. B., Twillie, A., Chadha, R., Patel, N. & Inaba, M. Dedifferentiating germ cells regain stem-cell specific polarity checkpoint prior to niche reentry. *bioRxiv*, 2023.2004.2026.538507 (2023). https://doi.org/10.1101/2023.04.26.538507
25 Sheng, X. R. & Matunis, E. Live imaging of the Drosophila spermatogonial stem cell niche reveals novel mechanisms regulating germline stem cell output. *Development* **138**, 3367-3376 (2011). https://doi.org/10.1242/dev.065797
26 Bener, M. B., Twillie, A. & Inaba, M. Dedifferentiating germ cells regain stem-cell specific polarity checkpoint prior to niche reentry. *bioRxiv*, 2023.2004.2026.538507 (2023). https://doi.org/10.1101/2023.04.26.538507
27 Gadre, P., Nitsure, N., Mazumdar, D., Gupta, S. & Ray, K. The rates of stem cell division determine the cell cycle lengths of its lineage. *iScience* **24**, 103232 (2021). https://doi.org/10.1016/j.isci.2021.103232
28 Ziehm, M., Piper, M. D. & Thornton, J. M. Analysing variation in Drosophila aging across independent experimental studies: a meta-analysis of survival data. *Aging Cell* **12**, 917-922 (2013). https://doi.org/10.1111/acel.12123

29 Jaiswal, S. & Ebert, B. L. Clonal hematopoiesis in human aging and disease. *Science* **366**, eaan4673 (2019). https://doi.org/doi:10.1126/science.aan4673
30 Jaiswal, S. *et al.* Clonal Hematopoiesis and Risk of Atherosclerotic Cardiovascular Disease. *N Engl J Med* **377**, 111-121 (2017). https://doi.org/10.1056/NEJMoa1701719
31 Zink, F. *et al.* Clonal hematopoiesis, with and without candidate driver mutations, is common in the elderly. *Blood* **130**, 742-752 (2017). https://doi.org/10.1182/blood-2017-02-769869
32 Oertel, M., Menthena, A., Dabeva, M. D. & Shafritz, D. A. Cell competition leads to a high level of normal liver reconstitution by transplanted fetal liver stem/progenitor cells. *Gastroenterology* **130**, 507-520; quiz 590 (2006). https://doi.org/10.1053/j.gastro.2005.10.049
33 van Neerven, S. M. *et al.* Apc-mutant cells act as supercompetitors in intestinal tumour initiation. *Nature* **594**, 436-441 (2021). https://doi.org/10.1038/s41586-021-03558-4
34 Flanagan, D. J. *et al.* NOTUM from Apc-mutant cells biases clonal competition to initiate cancer. *Nature* **594**, 430-435 (2021). https://doi.org/10.1038/s41586-021-03525-z
35 Fernandez-Antoran, D. *et al.* Outcompeting p53-Mutant Cells in the Normal Esophagus by Redox Manipulation. *Cell Stem Cell* **25**, 329-341.e326 (2019). https://doi.org/10.1016/j.stem.2019.06.011
36 Bajaj, J. *et al.* CD98-Mediated Adhesive Signaling Enables the Establishment and Propagation of Acute Myelogenous Leukemia. *Cancer Cell* **30**, 792-805 (2016). https://doi.org/10.1016/j.ccell.2016.10.003
37 McDermott, D. H. *et al.* Chromothriptic cure of WHIM syndrome. *Cell* **160**, 686-699 (2015). https://doi.org/10.1016/j.cell.2015.01.014
38 Menthena, A. *et al.* Activin A, p15INK4b signaling, and cell competition promote stem/progenitor cell repopulation of livers in aging rats. *Gastroenterology* **140**, 1009-1020 (2011). https://doi.org/10.1053/j.gastro.2010.12.003
39 Nichols, J., Lima, A. & Rodríguez, T. A. Cell competition and the regulative nature of early mammalian development. *Cell Stem Cell* **29**, 1018-1030 (2022). https://doi.org/https://doi.org/10.1016/j.stem.2022.06.003
40 Salzmann, V., Inaba, M., Cheng, J. & Yamashita, Y. M. Lineage tracing quantification reveals symmetric stem cell division in Drosophila male germline stem cells. *Cell Mol Bioeng* **6**, 441-448 (2013). https://doi.org/10.1007/s12195-013-0295-6
41 Gibson, M. A. & Bruck, J. Efficient Exact Stochastic Simulation of Chemical Systems with Many Species and Many Channels. *The Journal of Physical Chemistry A* **104**, 1876-1889 (2000). https://doi.org/10.1021/jp993732q
42 McHale, P. T. & Lander, A. D. The Protective Role of Symmetric Stem Cell Division on the Accumulation of Heritable Damage. *PLOS Computational Biology* **10**, e1003802 (2014). https://doi.org/10.1371/journal.pcbi.1003802
43 Shahriyari, L. & Komarova, N. L. Symmetric vs. Asymmetric Stem Cell Divisions: An Adaptation against Cancer? *PLOS ONE* **8**, e76195 (2013). https://doi.org/10.1371/journal.pone.0076195